arXiv:1401.3342v1 [astro-ph.SR] 14 Jan 2014

NPOI Measurements of Ten Stellar Oscillators

Ellyn K. Baines, J. Thomas Armstrong, Henrique R. Schmitt

Remote Sensing Division, Naval Research Laboratory, 4555 Overlook Avenue SW, Washington, DC 20375

ellyn.baines@nrl.navy.mil

James A. Benson, R. T. Zavala

U.S. Naval Observatory, Flagstaff Station, AZ 86001

Gerard T. van Belle

Lowell Observatory, Flagstaff, AZ 86001

ABSTRACT

Using the Navy Precision Optical Interferometer, we measured the angular diameters of 10 stars that have previously measured solar-like oscillations. Our sample covered a range of evolutionary stages but focused on evolved subgiant and giant stars. We combined our angular diameters with *Hipparcos* parallaxes to determine the stars' physical radii, and used photometry from the literature to calculate their bolometric fluxes, luminosities, and effective temperatures. We then used our results to test the scaling relations used by asteroseismology groups to calculate radii and found good agreement between the radii measured here and the radii predicted by stellar oscillation studies. The precision of the relations is not as well constrained for giant stars as it is for less evolved stars.

Subject headings: visible: stars, stars: fundamental parameters, techniques: interferometric)

1. Introduction

Asteroseismology, the study of stellar oscillations, is a powerful tool to infer information about stellar structure with minimal model dependence (see, e.g., Brown & Gilliland 1994; Christensen-Dalsgaard 2004). The frequencies of the observed oscillations depend on the sound speed inside the star, which in turn is dependent on properties of the interior

such as density, temperature, and gas motion (Carrier et al. 2010). The number of stars observed using asteroseismology and the quality of the data have increased dramatically in recent years, thanks to the photometric space missions *MOST* (*Microvariability and Oscillations of STars,* Walker et al. 2003), *CoRoT* (*Convection, Rotation, and planetary Transits,* Baglin et al. 2006; Auvergne et al. 2009), and *Kepler* (Borucki et al. 2010; Koch et al. 2010). The resulting stellar parameters are key to the statistical analysis of fundamental stellar properties and for testing stellar interior and evolutionary models (see, e.g., Chaplin et al. 2011).

Interferometry has the potential to make important contributions to asteroseismology, in part through the determinations of the targets' sizes (Cunha et al. 2007). Using interferometry, we can measure the angular diameters of stars with resolutions down to tenths of a milliarcsecond (see, e.g., Huber et al. 2012a; Baines et al. 2012). Once we know the apparent diameter of a star as well as its distance from parallax measurements, we can calculate its physical size. Then we can test the relationships used to derive stellar properties from asteroseismology observations by comparing the radii estimated using the asteroseismology relations to those measured interferometrically.

Huber et al. (2012b) presented interferometric diameters of 10 stars that had oscillation measurements from *CoRoT* and *Kepler*. They found an agreement between asteroseismic and interferometric radii of $\lesssim 4\%$ for dwarf stars and $\sim 13\%$ for giant stars. Their sample included five dwarf, one subgiant, and four giant stars. Here we focus on the more evolved stars: one dwarf, four subgiant, and five giant stars.

We observed these stars using the Navy Precision Optical Interferometer (NPOI) in order to measure their angular diameters. We then calculated their radii and effective temperatures, and used spectral energy distribution fits to determine their bolometric fluxes and luminosities. Section 2 discusses the NPOI and our observing process; Section 3 describes the visibility measurements and how we calculated various stellar parameters; Section 4 explores the relationship between radii determined using asteroseismology observations and radii measured interferometrically; and Section 5 summarizes our findings.

2. Interferometric Observations

The NPOI is an interferometer located on Anderson Mesa, AZ, and consists of two nested arrays: the four stations of the astrometric array (AC, AE, AW, and AN, which stand for astrometric center, east, west, and north, respectively) and the six stations of the imaging array, of which two stations are currently in operation (E6 and W7) and three more

will be coming online in the near future (E7, E10, and W10). The current baselines, i.e., the distances between the stations, range from 16 to 79 m, and our maximum baseline will be 432 m when the E10 and W10 stations are completed within the next year. We use a 12-cm region of the 50-cm siderostats and observe in 16 spectral channels spanning 550 to 850 nm simultaneously (Armstrong et al. 1998).

Each observation consisted of a 30–second coherent (on the fringe) scan in which the fringe contrast was measured every 2 ms, paired with an incoherent (off the fringe) scan used to estimate the additive bias affecting the visibility measurements (Hummel et al. 2003). Scans were taken on five baselines simultaneously. Each coherent scan was averaged to 1–second data points, and then to a single 30–second average. The dispersion of 1–second points provided an estimate of the internal uncertainties.

The target list was derived from the sample of stars with stellar oscillations that were bright enough to observing using the NPOI, which has a magnitude limit of $V = 6.5$. They also had to be resolved with the longest existing baseline, which gives a resolution limit of approximately 1 milliarcsecond (mas). This resulted in a list of 10 targets with stellar oscillation observations available to observe using the NPOI.

We interleaved data scans of the 10 asteroseismic targets with one to three calibrator stars for each target. Our calibrators are stars that are significantly less resolved on the baselines used than the targets. This meant that uncertainties in the calibrator's diameter did not affect the target's diameter calculation as much as if the calibrator star had a substantial angular size on the sky. The calibrator and target scans were measured as close in time and space as possible, which allowed us to convert instrumental target and calibrator visibilities to calibrated visibilities for the target. Preference was given to calibrators within 10° of the target stars, as was the case for 13 of the 16 calibrator stars used. On rare occasions, no suitable calibrator stars were within that angular distance so we resorted to stars that were more distant, with a maximum separation of 17°.

We estimated the calibrator stars' sizes by constructing their spectral energy distribution (SED) fits using photometric values published in Ljunggren & Oja (1965), McClure & Forrester (1981), Olsen (1993), Jasevicius et al. (1990), Golay (1972), Häggkvist & Oja (1970), Kornilov et al. (1991), Eggen (1968), Johnson et al. (1966), Cutri et al. (2003), and Gezari et al. (1993) as well as spectrophotometry from Glushneva et al. (1983), Glushneva et al. (1998), and Kharitonov et al. (1997) obtained via the interface created by Mermilliod et al. (1997). The assigned uncertainties for the 2MASS infrared measurements are as reported in Cutri et al. (2003), and an uncertainty of 0.05 mag was assigned to the optical measurements. We determined the best fit stellar spectral template to the photometry from the flux-calibrated stellar spectral atlas of Pickles (1998) using the χ^2 minimization technique (Press et al. 1992;

Wall & Jenkins 2003). The resulting calibrator angular diameter estimates are listed in Table 1.

3. Results

3.1. Angular Diameter Measurement

Interferometric diameter measurements use V^2, the square of the fringe visibility. For a point source, V^2 is unity, while for a uniformly-illuminated disk, $V^2 = [2J_1(x)/x]^2$, where J_1 is the Bessel function of the first order, $x = \pi B \theta_{\rm UD} \lambda^{-1}$, B is the projected baseline toward the star's position, $\theta_{\rm UD}$ is the apparent uniform disk angular diameter of the star, and λ is the effective wavelength of the observation (Shao & Colavita 1992). $\theta_{\rm UD}$ results are listed in Table 2. Our data files in OIFITS format are available upon request.

A more realistic model of a star's disk includes limb darkening (LD). If a linear LD coefficient μ_λ is used,

$$V^2 = \left(\frac{1-\mu_\lambda}{2} + \frac{\mu_\lambda}{3}\right)^{-1} \times \left[(1-\mu_\lambda)\frac{J_1(x_{\rm LD})}{x_{\rm LD}} + \mu_\lambda \left(\frac{\pi}{2}\right)^{1/2} \frac{J_{3/2}(x_{\rm LD})}{x_{\rm LD}^{3/2}}\right]. \quad (1)$$

where $x_{\rm LD} = \pi B \theta_{\rm LD} \lambda^{-1}$ (Hanbury Brown et al. 1974). We used effective temperature ($T_{\rm eff}$) and surface gravity ($\log g$) values from the literature with a microturbulent velocity of 2 km s^{-1} and to obtain μ_λ from Claret & Bloemen (2011). These values and the resulting $\theta_{\rm LD}$ are listed in Table 2. Figures 1 and 2 show the $\theta_{\rm LD}$ fits for all the stars. The two stars with the largest percent uncertainties in the $\theta_{\rm LD}$ fit (2%) are HD 146791 and HD 181907. This is because their visibility curves are less well sampled with respect to spatial frequency than the other targets.

Seven of the 10 stars measured here had previous interferometric diameter measurements. They are listed in Table 3 and are plotted against our values in Figure 3. In all cases but one, the uncertainty on our diameter measurement is smaller than those from the literature, and they all agree to within 3-σ.

The uncertainty for the $\theta_{\rm LD}$ fit was derived using the method described in Tycner et al. (2010), who showed that a non-linear least-squares method does not sufficiently account for atmospheric effects on time scales shorter than the window between target and calibrator observations. They describe a bootstrap Monte Carlo method that treats the observations as groups of data points because the NPOI collects data in scans consisting of 16 channels

simultaneously.[1] They discovered that when the 16 data points were analyzed individually, a single scan's deviation from the trend had a large impact on the resulting diameter and uncertainty calculation. On the other hand, when they preserved the inherent structure of the observational data by using the groups of 16 channels instead of individual data points, the uncertainty on the angular diameter was larger and more realistic. This method makes no assumptions about underlying uncertainties due to atmospheric effects, which are applicable to all stars observed using ground–based instruments. It should be noted that the number of calibrator stars used in the observations have no apparent effect on the $\theta_{\rm LD}$ fit uncertainty.

3.2. Stellar Radius, Luminosity and Effective Temperature

For each star, the parallax from van Leeuwen (2007) was converted into a distance, which we then combined with our measured $\theta_{\rm LD}$ to calculate the linear radius (R). In order to determine the luminosity (L) and $T_{\rm eff}$, we constructed each star's SED using the sources and technique of fitting spectral templates to observed photometry as described in Section 2. The resulting SED gave us the bolometric flux ($F_{\rm BOL}$) and allowed for the calculation of extinction $A_{\rm V}$ with the wavelength-dependent reddening relations of Cardelli et al. (1989).

We combined our $F_{\rm BOL}$ values with the stars' distances to estimate L using $L = 4\pi d^2 F_{\rm BOL}$. We also combined the $F_{\rm BOL}$ with $\theta_{\rm LD}$ to determine each star's effective temperature by inverting the relation,

$$F_{\rm BOL} = \frac{1}{4}\theta_{\rm LD}^2 \sigma T_{\rm eff}^4, \tag{2}$$

where σ is the Stefan-Boltzmann constant and $\theta_{\rm LD}$ is in radians.

Because μ_λ is chosen based on a given $T_{\rm eff}$, we checked to see if μ_λ and therefore $\theta_{\rm LD}$ would change based on our new $T_{\rm eff}$. In most cases, μ_λ changed by 0.0 or 0.01, and the largest difference was 0.08 for HD 181907. The resulting $\theta_{\rm LD}$ values changed at most by 1%, and all but three changed by 0.2% or less. This was well within the uncertainties on $\theta_{\rm LD}$, and re-calculating $T_{\rm eff}$ with the new $\theta_{\rm LD}$ made at most a 26 K difference (for HD 181907, which has an uncertainty of 199 K). These values all converged after this one iteration, and these are the final numbers listed in Table 2.

[1]For every "scan," 30 seconds of data are collected in each of the 16 wavelength channels with a measurement once every 2 milliseconds. During the processing described in Section 2, all the 30-second-scan's data points are averaged into one data point for each channel, so we go from 30 seconds of data per channel to one averaged data point per channel.

4. Discussion

Two scaling equations relate observed asteroseismic quantities to fundamental stellar parameters:

$$\Delta\nu \propto M^{\frac{1}{2}} R^{-\frac{3}{2}}, \tag{3}$$

where $\Delta\nu$ is the large separation of oscillation modes of the same degree and consecutive orders and M is the mass of the star (Ulrich 1986), and

$$\nu_{\rm max} \propto M R^{-2} T_{\rm eff}^{-\frac{1}{2}}, \tag{4}$$

where $\nu_{\rm max}$ is the frequency of maximum oscillation power (Brown et al. 1991; Kjeldsen & Bedding 1995). These equations are often used to calculate stellar radii and masses from oscillation observations. However, when R is measured interferometrically, we can test the relations themselves.

We used $\Delta\nu$ and $\nu_{\rm max}$ from the references listed in Table 4 and assumed uncertainties of 1% in $\Delta\nu$ and 3% in $\nu_{\rm max}$ (Huber et al. 2012b) when no uncertainties were provided in the references. We combined the frequency measurements with effective temperatures from the literature ($T_{\rm lit}$) to calculate R from the asteroseismic measurements alone. It should be noted that the $T_{\rm lit}$ used has little impact on $\nu_{\rm max}$. A variation of 100 K causes a 0.9% change in $\nu_{\rm max}$, which is typically on the order of or smaller than the uncertainties in $T_{\rm lit}$ (Huber et al. 2012b).

Table 4 and Figure 4 show the results comparing the radii calculated from asteroseismology ($R_{\rm a}$) and those measured using interferometry ($R_{\rm i}$). The stars with the largest difference between the two are HD 153210, HD 161797, and HD 168723. For the latter two stars, previously published angular diameters agree with our measurement to 1% or less. HD 153210 has not been previously measured, and our diameter agrees with that predicted by the SED within 2-σ. For the remaining stars, $R_{\rm a}$ and $R_{\rm i}$ agree within 3-σ ($\sim$ 10%) in all cases except for HD 146791 and HD 150680, which agree within 4-σ ($\sim$ 15%). Three of the others (HD 163588, HD 181907, and HD 188512) agree within 1-σ (1 to 2%).

Barban et al. (2004) quote a range for $\nu_{\rm max}$ between 80 and 170 μHz for HD 168723, and Stello et al. (2009) lists a value of 130 μHz. If we use 130 μHz in our calculation for $R_{\rm a}$, the result is 12.08$\pm$0.44 $R_\odot$, which is approximately twice the value of $R_{\rm i}$ = 5.92$\pm$0.02 $R_\odot$. However, if we use the lower end of the range, i.e., 80 μHz, $R_{\rm a}$ is 7.43$\pm$0.27 $R_\odot$, which is still a 26% difference from the one presented here. We believe further asteroseismic observations

of this star would be particularly interesting.

Some stars have more evenly and completely sampled data along the visibility curves than others; for example, HD 146791 and HD 181907 do not have as wide a range of measurements as a function of spatial frequency that other stars such as HD 121370 and HD 153210 display. We considered whether or not this would have an effect on the scatter in Figure 4 but the stars with sparsely sampled curves do not correspond to the outliers, so that is not the issue. In general, we do not observe any systematic trend as a function of size. The residual scatter in the giant stars is comparable to what Huber et al. (2012b) found, and shows the relationships between observed $\Delta\nu$ and $\nu_{\rm max}$ and stellar radii are not as precise for evolved giant stars as they are for dwarf stars.

The scaling relation for $\nu_{\rm max}$ is considered to be less robust than the relation for $\Delta\nu$ (Huber et al. 2012b), so we wanted to test it. We combined Equation (3) with our $R_{\rm i}$ to calculate stellar masses, and then combined the masses with our new $T_{\rm eff}$ to calculate $\nu_{\rm max}$ values and compare them to the measured values. Table 4 lists and Figure 5 shows the results. The largest outliers are again HD 153210, HD 161797, and HD 168723 due to the discrepancies in calculated radii described above. HD 150680 also shows a 16% difference between the observed and calculated $\nu_{\rm max}$ value. Our angular diameter for this star matches those measured by Nordgren et al. (2001) and Mozurkewich et al. (2003) to within 3-σ, and it only differs from the SED estimate by 3%. We note that the mass listed in Kallinger et al. (2009) is 1.19 $M_{\odot}$ while the mass determined by Martić et al. (2001) is 1.3 to 1.5 $M_{\odot}$. The latter agrees with the mass determined using our interferometric radius measurement: 1.33±0.04 $M_{\odot}$. In general we observe good agreement between the observed and calculated $\nu_{\rm max}$ within the uncertainty bars with no systematics with respect to stellar size or evolutionary status.

5. Summary

We measured the angular diameters of 10 stars using the NPOI. The combination of these observations with other information from the literature allowed us to calculate the stars' R, $T_{\rm eff}$, $F_{\rm BOL}$, and L. We compared our interferometric radius $R_{\rm i}$ values to those determined from asteroseismic scaling relations and found good agreement between the two, particularly for the less evolved stars. Then we also used $\Delta\nu$ from the literature and our $R_{\rm i}$ to calculate the stars' masses and $\nu_{\rm max}$ to put that scaling relation to the test as well. Again, the results agreed to within a few σ in general.

The relations work best for main-sequence stars and have limited precision for giant

stars. Hopefully future observations with planned spacecraft such as *Gaia* (Perryman 2003) and *TESS* (Transiting Exoplanet Survey Satellite, Ricker et al. 2009) as well as planned upgrades to existing interferometers such as the addition of longer baselines on the NPOI (increased resolution), new hardware (increased magnitude limit), and the eventual addition of large telescopes to the array (see, e.g., Armstrong et al. 2013) will lead to significant improvements when combining data from two techniques.

The Navy Precision Optical Interferometer is a joint project of the Naval Research Laboratory and the U.S. Naval Observatory, in cooperation with Lowell Observatory, and is funded by the Office of Naval Research and the Oceanographer of the Navy. This research has made use of the SIMBAD database, operated at CDS, Strasbourg, France. This publication makes use of data products from the Two Micron All Sky Survey, which is a joint project of the University of Massachusetts and the Infrared Processing and Analysis Center/California Institute of Technology, funded by the National Aeronautics and Space Administration and the National Science Foundation.

REFERENCES

Absil, O., Defrère, D., Coudé du Foresto, V., et al. 2013, A&A, 555, A104

Ammons, S. M., Robinson, S. E., Strader, J., et al. 2006, ApJ, 638, 1004

Armstrong, J. T., Mozurkewich, D., Rickard, L. J, et al. 1998, ApJ, 496, 550

Armstrong, J. T., Hutter, D. J., Baines, E. K., et al. 2013, Journal of Astronomical Instrumentation, in press

Auvergne, M., Bodin, P., Boisnard, L., et al. 2009, A&A, 506

Baglin, A., Michel, E., Auvergne, M., & COROT Team 2006, Proceedings of SOHO 18/GONG 2006/HELAS I, Beyond the spherical Sun, 624

Baines, E. K., White, R. J., Huber, D., et al. 2012, ApJ, 761, 57

Barban, C., De Ridder, J., Mazumdar, A., et al. 2004, SOHO 14 Helio- and Asteroseismology: Towards a Golden Future, 559, 113

Barban, C., Matthews, J. M., De Ridder, J., et al. 2007, A&A, 468, 1033

Bonanno, A., Benatti, S., Claudi, R., et al. 2008, ApJ, 676, 1248

Borucki, W. J., Koch, D., Basri, G., et al. 2010, Science, 327, 977

Brown, T. M., Gilliland, R. L., Noyes, R. W., & Ramsey, L. W. 1991, ApJ, 368, 599

Brown, T. M., & Gilliland, R. L. 1994, ARA&A, 32, 37

Cardelli, J. A., Clayton, G. C., & Mathis, J. S. 1989, ApJ, 345, 245

Carrier, F., Eggenberger, P., & Bouchy, F. 2005, A&A, 434, 1085

Carrier, F., De Ridder, J., Baudin, F., et al. 2010, A&A, 509, A73

Chaplin, W. J., Kjeldsen, H., Christensen-Dalsgaard, J., et al. 2011, Science, 332, 213

Christensen-Dalsgaard, J. 2004, Sol. Phys., 220, 137

Claret, A., & Bloemen, S. 2011, A&A, 529, A75

Corsaro, E., Grundahl, F., Leccia, S., et al. 2012, A&A, 537, A9

Cunha, M. S., Aerts, C., Christensen-Dalsgaard, J., et al. 2007, A&A Rev., 14, 217

Cutri, R. M., et al. 2003, The IRSA 2MASS All-Sky Point Source Catalog, NASA/IPAC Infrared Science Archive

di Folco, E., Absil, O., Augereau, J.-C., et al. 2007, A&A, 475, 243

Eggen, O. J. 1968, London, H.M.S.O., 1968

Gezari, D. Y., Schmitz, M., Pitts, P. S., & Mead, J. M. 1993, Unknown

Glushneva, I. N., Doroshenko, V. T., Fetisova, T. S., et al. 1983, Trudy Gosudarstvennogo Astronomicheskogo Instituta, 53, 50

Glushneva, I. N., Doroshenko, V. T., Fetisova, T. S., et al. 1998, VizieR Online Data Catalog, 3207, 0

Golay, M. 1972, Vistas in Astronomy, 14, 13

Häggkvist, L., & Oja, T. 1970, A&AS, 1, 199

Hanbury Brown, R., Davis, J., Lake, R. J. W., & Thompson, R. J. 1974, MNRAS, 167, 475

Huber, D., Ireland, M. J., Bedding, T. R., et al. 2012a, MNRAS, 423, L16

Huber, D., Ireland, M. J., Bedding, T. R., et al. 2012b, ApJ, 760, 32

Hummel, C. A., Benson, J. A., Hutter, D. J., et al. 2003, AJ, 125, 2630

Jasevicius, V., Kuriliene, G., Strazdaite, V., et al. 1990, Vilnius Astronomijos Observatorijos Biuletenis, 85, 50

Johnson, H. L., Mitchell, R. I., Iriarte, B., & Wisniewski, W. Z. 1966, Communications of the Lunar and Planetary Laboratory, 4, 99

Kallinger, T., Weiss, W. W., De Ridder, J., Hekker, S., & Barban, C. 2009, The Eighth Pacific Rim Conference on Stellar Astrophysics: A Tribute to Kam-Ching Leung, 404, 307

Kharitonov, A. V., Tereshchenko, V. M., & Knyazeva, L. N. 1997, VizieR Online Data Catalog, 3202, 0

Kjeldsen, H., & Bedding, T. R. 1995, A&A, 293, 87

Koch, D. G., Borucki, W. J., Basri, G., et al. 2010, ApJ, 713, L79

Kornilov, V. G., Volkov, I. M., Zakharov, A. I., et al. 1991, Trudy Gosudarstvennogo Astronomicheskogo Instituta, 63, 1

Ljunggren, B., & Oja, T. 1965, Arkiv for Astronomi, 3, 439

Martić, M., Lebrun, J. C., Schmitt, J., Appourchaux, T., & Bertaux, J. L. 2001, SOHO 10/GONG 2000 Workshop: Helio- and Asteroseismology at the Dawn of the Millennium, 464, 431

Mazumdar, A., Mérand, A., Demarque, P., et al. 2009, A&A, 503, 521

McClure, R. D., & Forrester, W. T. 1981, Publications of the Dominion Astrophysical Observatory Victoria, 15, 439

Mérand, A., Kervella, P., Barban, C., et al. 2010, A&A, 517, A64

Mermilliod, J.-C., Mermilliod, M., & Hauck, B. 1997, A&AS, 124, 349

Morel, T., & Miglio, A. 2012, MNRAS, 419, L34

Mozurkewich, D., Armstrong, J. T., Hindsley, R. B., et al. 2003, AJ, 126, 2502

Nordgren, T. E., Germain, M. E., Benson, J. A., et al. 1999, AJ, 118, 3032

Nordgren, T. E., Sudol, J. J., & Mozurkewich, D. 2001, AJ, 122, 2707

Olsen, E. H. 1993, A&AS, 102, 89

Perryman, M. A. C. 2003, GAIA Spectroscopy: Science and Technology, 298, 3

Pickles, A. J. 1998, PASP, 110, 863

Pijpers, F. P., Teixeira, T. C., Garcia, P. J., et al. 2003, A&A, 406, L15

Press, W. H., Teukolsky, S. A., Vetterling, W. T., & Flannery, B. P. 1992, Numerical recipes in C. The art of scientific computing (Cambridge: University Press, c1992, 2nd ed.)

Prugniel, P., Soubiran, C., Koleva, M., & Le Borgne, D. 2007, arXiv:astro-ph/0703658

Prugniel, P., Vauglin, I., & Koleva, M. 2011, A&A, 531, A165

Ricker, G. R., Latham, D. W., Vanderspek, R. K., et al. 2009, American Astronomical Society Meeting Abstracts #214, 214, #306.05

Shao, M., & Colavita, M. M. 1992, ARA&A, 30, 457

Stello, D., Chaplin, W. J., Basu, S., Elsworth, Y., & Bedding, T. R. 2009, MNRAS, 400, L80

Teixeira, T. C., Kjeldsen, H., Bedding, T. R., et al. 2009, A&A, 494, 237

Thévenin, F., Kervella, P., Pichon, B., et al. 2005, A&A, 436, 253

Tycner, C., Hutter, D. J., & Zavala, R. T. 2010, Proc. SPIE, 7734, 103T

Ulrich, R. K. 1986, ApJ, 306, L37

van Leeuwen, F. 2007, A&A, 474, 653

Walker, G., Matthews, J., Kuschnig, R., et al. 2003, PASP, 115, 1023

Wall, J. V., & Jenkins, C. R. 2003, Practical Statistics for Astronomers (Princeton Series in Astrophysics)

Wu, Y., Singh, H. P., Prugniel, P., Gupta, R., & Koleva, M. 2011, A&A, 525, A71

This preprint was prepared with the AAS LaTeX macros v5.2.

Table 1. Observing Log and Calibrator Stars' Angular Diameters.

Target HD	Other Name	Calibrator HD	Date (UT)	Baselines Used†	# Obs	$\theta_{\rm LD,cal}$ (mas)
10700	τ Cet	11171	2005/09/17	AC-W7, AE-W7	19	0.682±0.034
			2005/09/18	AC-W7	9	
			2005/09/25	AC-W7, AE-W7	44	
121370	η Boo	122408	2012/05/10	AW-E6, E6-W7	126	0.521±0.026
			2012/05/11	AE-AW, E6-W7	90	
			2012/05/12	E6-W7	27	
			2012/05/15	AW-E6, E6-W7	108	
146791	ϵ Oph	141513	2010/03/21	AW-W7	30	0.524±0.026
			2010/03/28	AW-W7	13	
150680	ζ Her	156164	2005/08/18	AE-W7, E6-W7	50	0.887±0.044
			2005/08/25	AC-W7, AE-W7, E6-W7	120	
153210	κ Oph	148112	2013/02/23	AC-AE, AC-AW, AC-E6	18	0.443±0.022
			2013/03/01	AC-AW	12	
			2013/03/02	AC-E6, AW-E6	63	
			2013/03/05	AC-E6, AW-E6	198	
			2013/03/06	AC-E6, AW-E6	72	
			2013/03/07	AC-E6, AW-E6	90	
		152614	2013/02/23	AC-E6, AC-AW	34	0.316±0.016
			2013/02/25	AC-E6	14	
			2013/03/02	AC-E6, AW-E6	90	
			2013/03/05	AC-E6, AW-E6	261	
			2013/03/07	AC-E6, AW-E6	63	
			2013/04/01	AE-E6, AW-E6	53	
			2013/04/02	AE-E6, AW-E6	35	
			2013/04/03	AE-E6, AW-E6	54	
		147547	2013/04/19	AE-AW, AW-E6	68	0.970±0.049
			2013/04/22	AE-E6, AW-E6	115	
			2013/04/23	AE-E6, AW-E6	91	
			2013/04/26	AE-E6, AW-E6	165	

Table 1—Continued

Target HD	Other Name	Calibrator HD	Date (UT)	Baselines Used†	# Obs	$\theta_{\rm LD,cal}$ (mas)
161797	μ Her	166014	2010/08/21	AE-AW, AW-E6	270	0.596±0.030
			2010/08/26	AE-AW, AW-E6	58	
163588	ξ Dra	159541	2013/04/27	AE-AW, AW-E6	18	0.520±0.026
			2013/04/28	AW-E6	43	
			2013/04/29	AE-AW, AW-E6	97	
		168151	2013/04/27	AE-AW, AW-E6	43	0.655±0.033
			2013/04/28	AE-AW, AW-E6	49	
			2013/04/29	AE-AW, AW-E6	90	
			2013/05/01	AW-E6	10	
			2013/05/03	AE-AW	12	
			2013/05/09	AW-E6	170	
			2013/05/12	AW-E6	23	
			2013/05/13	AW-E6	236	
			2013/05/14	AE-AW	32	
		184006	2013/05/01	AW-E6	32	0.703±0.035
			2013/05/12	AE-AW, AW-E6	48	
			2013/05/13	AW-E6	104	
			2013/05/14	AE-AW	49	
168723	η Ser	161868	2004/05/20	AC-AE, AC-AW	90	0.668±0.033
			2004/05/24	AC-AE, AC-AW	17	
		164353	2007/05/18	AW-E6, E6-W7	120	0.371±0.022
			2007/05/24	AN-E6, AW-E6, E6-W7	278	
			2007/05/25	AN-E6, AW-E6	20	
			2007/05/31	AW-E6, E6-W7	128	
181907	HR 7349	177756	2013/05/21	AW-E6	62	0.571±0.029
			2013/05/31	AC-AW, AW-E6	16	
			2013/06/03	AW-E6	23	
			2013/06/05	AW-E6	10	
		184930	2013/05/21	AW-E6	71	0.311±0.016

Table 1—Continued

Target HD	Other Name	Calibrator HD	Date (UT)	Baselines Used†	# Obs	$\theta_{\rm LD,cal}$ (mas)
			2013/05/31	AC-AW, AW-E6	16	
			2013/06/03	AW-E6	21	
			2013/06/05	AW-E6	10	
188512	β Aql	195810	2007/05/26	AN-AW, AW-W7	14	0.394±0.020
			2007/05/30	AW-E6, E6-W7	57	
			2007/05/31	AN-E6, AW-E6, E6-W7	219	
			2007/06/04	AW-E6, E6-W7	140	
			2007/06/09	AN-E6, AW-E6, E6-W7	120	
			2007/06/11	AW-E6, E6-W7	89	

Note. — †The maximum baseline lengths are AC-AE 18.9 m, AC-AW 22.2 m, AC-E6 34.4 m, AC-W7 51.3 m, AE-AW 37.5 m, AE-W7 64.2 m, AN-AW 38.2 m, AN-E6 45.6 m, AW-E6 53.3 m, AW-W7 29.5 m, and E6-W7 79.4 m. The $\theta_{\rm LD,cal}$ estimates were determined using the technique described in Section 2.

Table 2. Stellar Parameters.

Target HD	Spectral Type	Parallax (mas)	μ_λ	$\theta_{\rm UD}$ (mas)	$\theta_{\rm LD}$ (mas)	$\sigma_{\rm LD}$ (%)	# Cals	$R_{\rm linear}$ ($R_\odot$)	L ($L_\odot$)	$F_{\rm BOL}$ (10^{-8} erg s^{-1} cm^{-2})	$T_{\rm eff}$ (K)	$\sigma_{\rm Teff}$ %
10700	G8.5 V	273.96±0.17	0.60	1.952±0.003	2.072±0.010	0.5	1	0.81±0.01	0.47±0.01	113.0±0.3	5301±13	0.2
121370	G0 IV	87.75±1.24	0.52	2.023±0.002	2.134±0.012	0.6	1	2.61±0.04	8.69±0.25	214.0±0.7	6128±18	0.3
146791	G9.5 III	30.64±0.20	0.65	2.772±0.007	2.966±0.061	2.1	1	10.40±0.22	56.64±1.29	170.0±3.2	4907±55	1.1
150680	G0 IV	93.32±0.47	0.53	2.175±0.001	2.266±0.014	0.6	1	2.61±0.02	8.12±0.08	226.0±0.6	6029±19	0.3
153210	K2 III	35.66±0.20	0.71	3.479±0.001	3.657±0.013	0.4	3	11.02±0.07	50.67±1.14	206.0±4.0	4367±24	0.5
161797	G5 IV	123.33±0.16	0.58	1.851±0.002	1.957±0.012	0.6	1	1.71±0.01	2.10±0.01	102.0±0.2	5317±16	0.3
163588	K2 III	28.98±0.12	0.70	2.894±0.002	3.116±0.008	0.3	3	11.56±0.06	47.30±0.44	127.0±0.6	4451±7	0.2
168723	K0 III-IV	53.93±0.18	0.65	2.852±0.001	2.970±0.007	0.2	2	5.92±0.02	17.85±0.13	166.0±0.4	4875±7	0.1
181907	G8 III	9.67±0.34	0.67	1.038±0.009	1.089±0.023	2.1	2	12.10±0.50	96.68±16.0	29.5±4.3	5227±199	3.8
188512	G9.5 IV	78.00±0.20	0.63	2.042±0.001	2.166±0.009	0.4	1	2.98±0.01	4.99±0.03	97.1±0.2	4992±11	0.2

Note. — The parallaxes are from van Leeuwen (2007); the μ_λ coefficients are from Claret & Bloemen (2011) in the R-band with a microturbulent velocity of 2 km s^{-1}. The sources of $T_{\rm eff}$ and log g used to determine μ_λ were the following: Prugniel et al. (2011) for HD 10700, HD 121370, HD 161797, HD 168723, and HD 188512; Wu et al. (2011) for HD 146791 and HD 163588; Prugniel et al. (2007) for HD 150680; Morel & Miglio (2012) for HD 153210; and Ammons et al. (2006) for HD 181907.

Table 3. Angular Diameter Comparison.

Target HD	$\theta_{\rm LD,thiswork}$ (mas)	$\theta_{\rm LD,SED}$ (mas)	% diff	$\theta_{\rm LD,previous}$ (mas)	Reference	% diff
10700	2.072±0.010	2.047±0.038	1	1.97±0.05	Pijpers et al. (2003)	5
				2.015±0.011	di Folco et al. (2007)	3
121370	2.134±0.012	2.280±0.069	7	2.28±0.07	Nordgren et al. (2001)	7
				2.269±0.025	Mozurkewich et al. (2003)	6
				2.200±0.027	Thévenin et al. (2005)	3
146791	2.966±0.061	3.031±0.165	2	2.961±0.007	Mazumdar et al. (2009)	0.2
150680	2.266±0.014	2.342±0.071	3	2.49±0.09	Nordgren et al. (2001)	10
				2.367±0.051	Mozurkewich et al. (2003)	4
153210	3.657±0.013	3.960±0.199	8	N/A	N/A	–
161797	1.957±0.012	1.767±0.051	10	1.953±0.039	Mozurkewich et al. (2003)	0.2
				1.975±0.025	Absil et al. (2013)	1
163588	3.116±0.008	3.114±0.154	0.1	N/A	N/A	–
168723	2.970±0.007	2.993±0.160	1	2.944±0.010	Mérand et al. (2010)	1
181907	1.089±0.023	1.185±0.112	8	N/A	N/A	–
188512	2.166±0.009	1.915±0.054	12	2.18±0.09	Nordgren et al. (1999)	1

Note. — The SED fit was created using the method described in Section 3.2. If more than one diameter is available in the literature, we used the most recent one when plotting the results in Figure 3.

Table 4. Comparing Interferometric and Asteroseismic Results.

Target HD	$T_{\rm i}$ (K)	$T_{\rm lit}$ (K)	$R_{\rm i}$ ($R_\odot$)	$R_{\rm a}$ ($R_\odot$)	% diff	$\Delta\nu$ (μHz)	$\nu_{\rm max}$ (μHz)	Reference	M ($M_\odot$)	$\nu_{\rm max,calc}$ (μHz)	% diff
10700	5301±13	5348±45	0.81±0.01	0.90±0.03	12	169	4500	Teixeira et al. (2009)	0.84±0.02	4062±108	10
121370	6128±18	5967±45	2.61±0.04	2.86±0.10	9	39.9±0.1	750	Carrier et al. (2005)	1.56±0.07	677±37	10
146791	4907±55	4918±28	10.40±0.22	11.76±0.43	13	5.3±0.1	60	Barban et al. (2007)	1.74±0.13	53±5	11
150680	6029±19	5758±81	2.61±0.02	3.05±0.11	17	37.01	701[a]	Kallinger et al. (2009)	1.34±0.04	586±21	16
153210	4637±24	4559±116	11.02±0.07	9.16±0.35	16	4.5	35	Stello et al. (2009)	1.49±0.04	42±1	19
161797	5317±16	5454±35	1.71±0.01	2.18±0.08	28	56.5±0.07	1200	Bonanno et al. (2008)	0.87±0.02	951±22	21
163588	4451±7	4483±25	11.56±0.06	11.83±0.43	2	4	36	Stello et al. (2009)	1.36±0.03	35±1	2
168723	4875±7	4923±63	5.92±0.02	7.43±0.27	26	7.7	80	Barban et al. (2004)	0.68±0.02	64±2	20
181907	5227±199	5637±228	12.10±0.50	12.01±0.52	1	3.47±0.12	27[b]	Carrier et al. (2010)	1.17±0.17	26±4	5
188512	4992±11	5082±69	2.98±0.01	3.02±0.11	1	29.56±0.10	472±72	Corsaro et al. (2012)	1.28±0.02	470±9	0.4

Note. — $T_{\rm i}$ is the interferometrically calculated effective temperature from Table 2; $T_{\rm lit}$ is the effective temperature from the literature as listed in Table 2. $R_{\rm i}$ is the interferometrically measured radius; $R_{\rm a}$ is the radius calculated using $\nu_{\rm max}$ and $\Delta\nu$ from asteroseismic observations as well as $T_{\rm lit}$; $\nu_{\rm max}$ and $\Delta\nu$ are from the references listed; M is the mass calculated using $\Delta\nu$ and $R_{\rm i}$; and $\nu_{\rm max,calc}$ is the $\nu_{\rm max}$ calculated using M and $T_{\rm i}$.

[a]No $\nu_{\rm max}$ was listed, so it was calculated using $T_{\rm eff}$ from Martić et al. (2001) and M and R from Kallinger et al. (2009).

[b]No $\nu_{\rm max}$ was listed, so it was calculated using $T_{\rm eff}$, M, and R from Carrier et al. (2010).

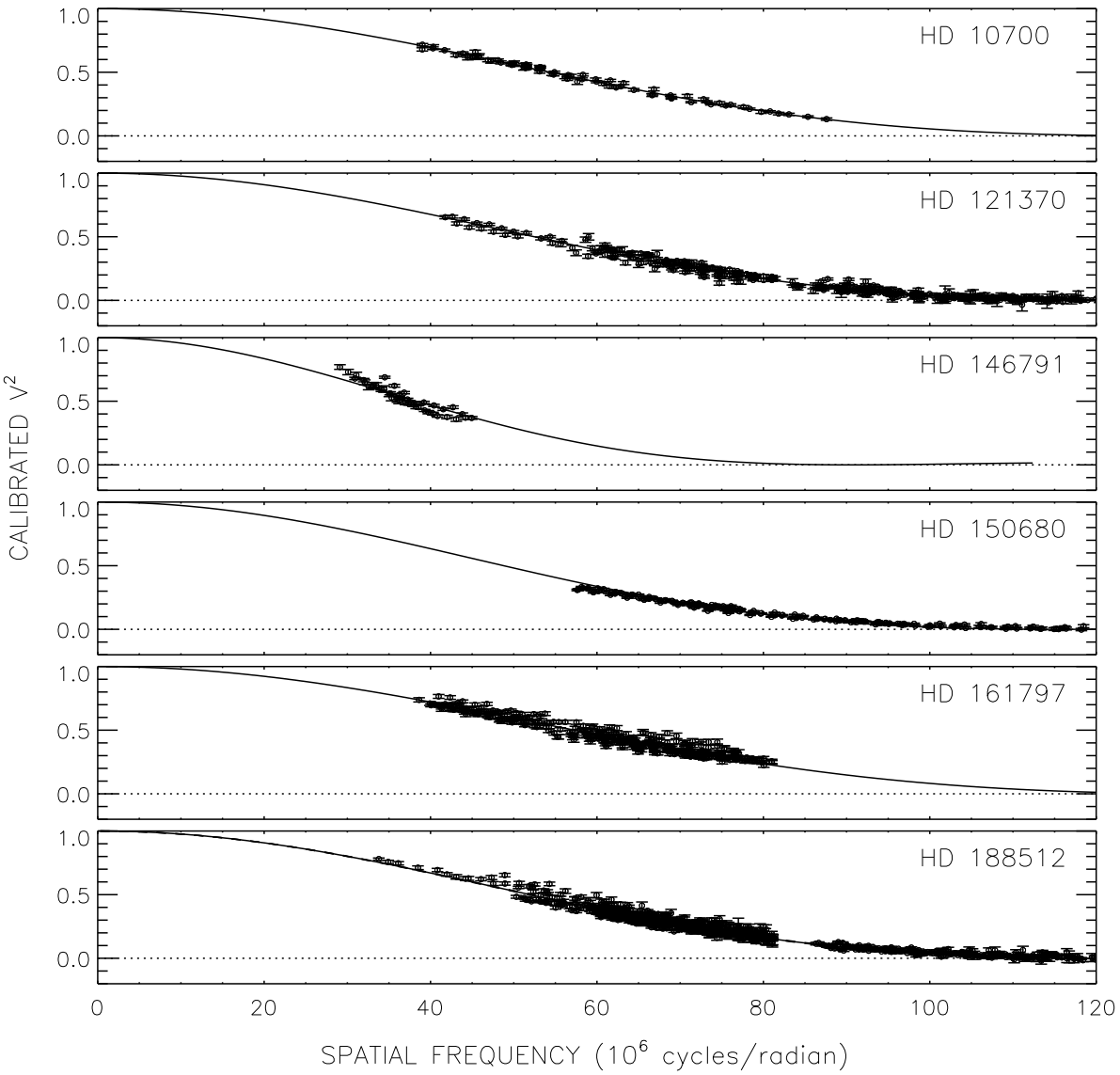

Fig. 1.— $\theta_{\rm LD}$ fits for stars observed with one calibrator. The solid lines represent the theoretical visibility curve for the best fit $\theta_{\rm LD}$, the points are the calibrated visibilities, and the vertical lines are the measurement uncertainties. The uncertainty in the $\theta_{\rm LD}$ fit is not shown because it largely indistinguishable from the best fit $\theta_{\rm LD}$ curve on this scale. See Table 2 for the uncertainty.

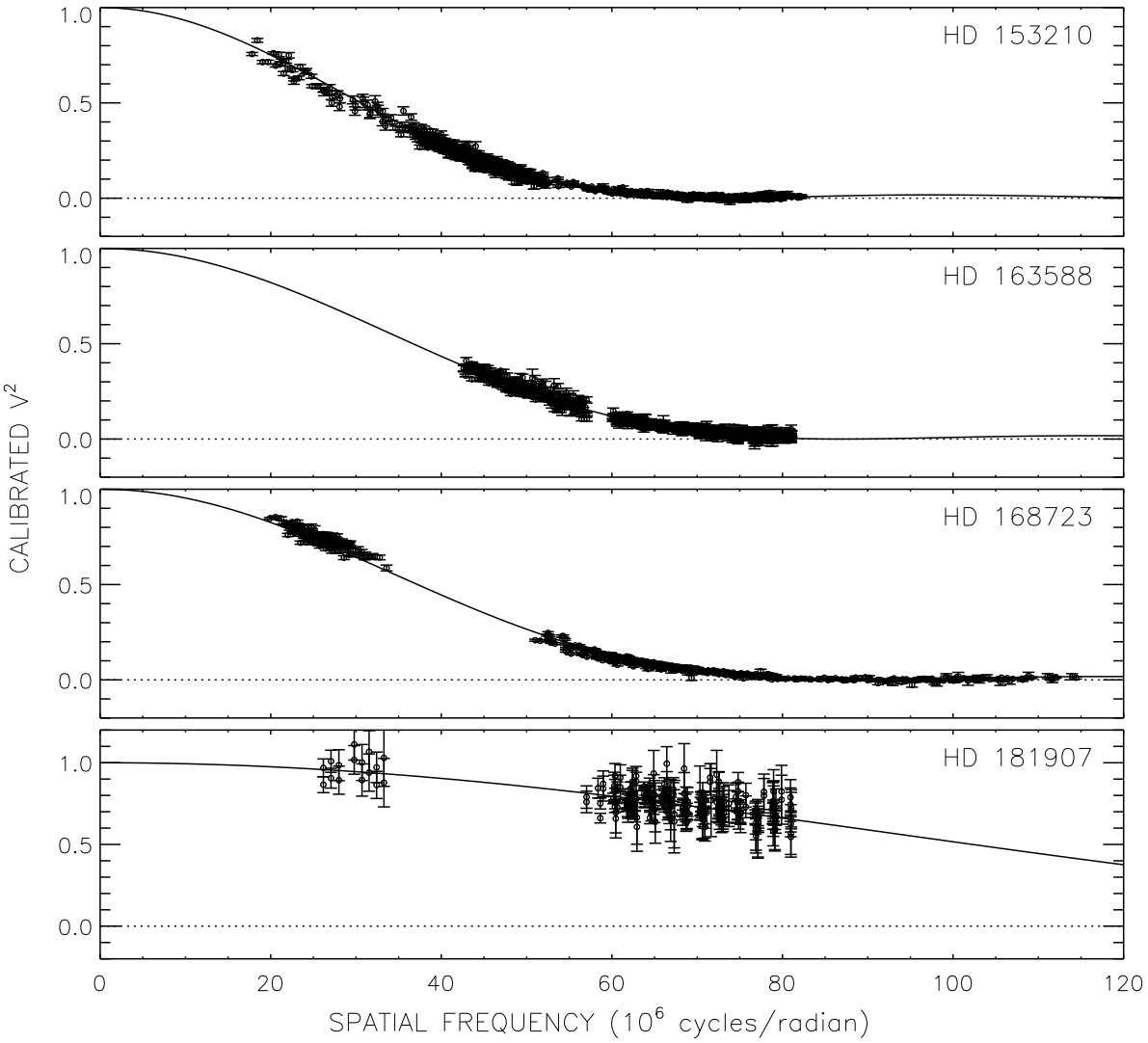

Fig. 2.— $\theta_{\rm LD}$ fits for stars observed with two or three calibrators. The symbols are the same as in Figure 1.

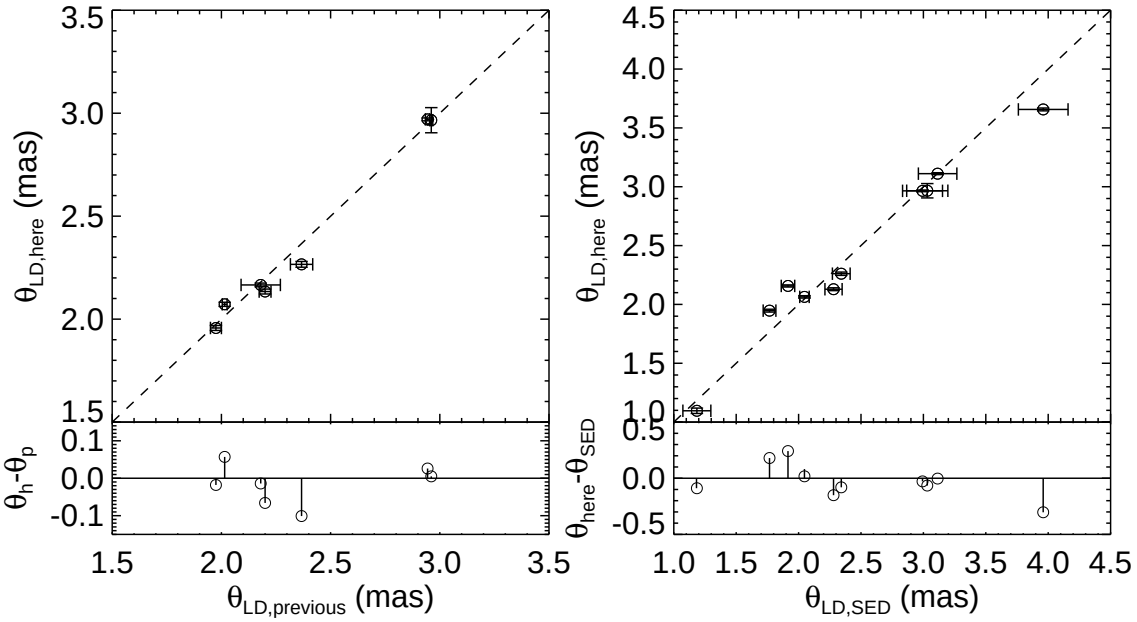

Fig. 3.— Comparison between $\theta_{\rm LD}$ measured here and previous interferometric measurements from the literature (left panel) and compared to SED fits (right panel). The bottom panels show the residuals to the fit. The values used are listed in Table 3.

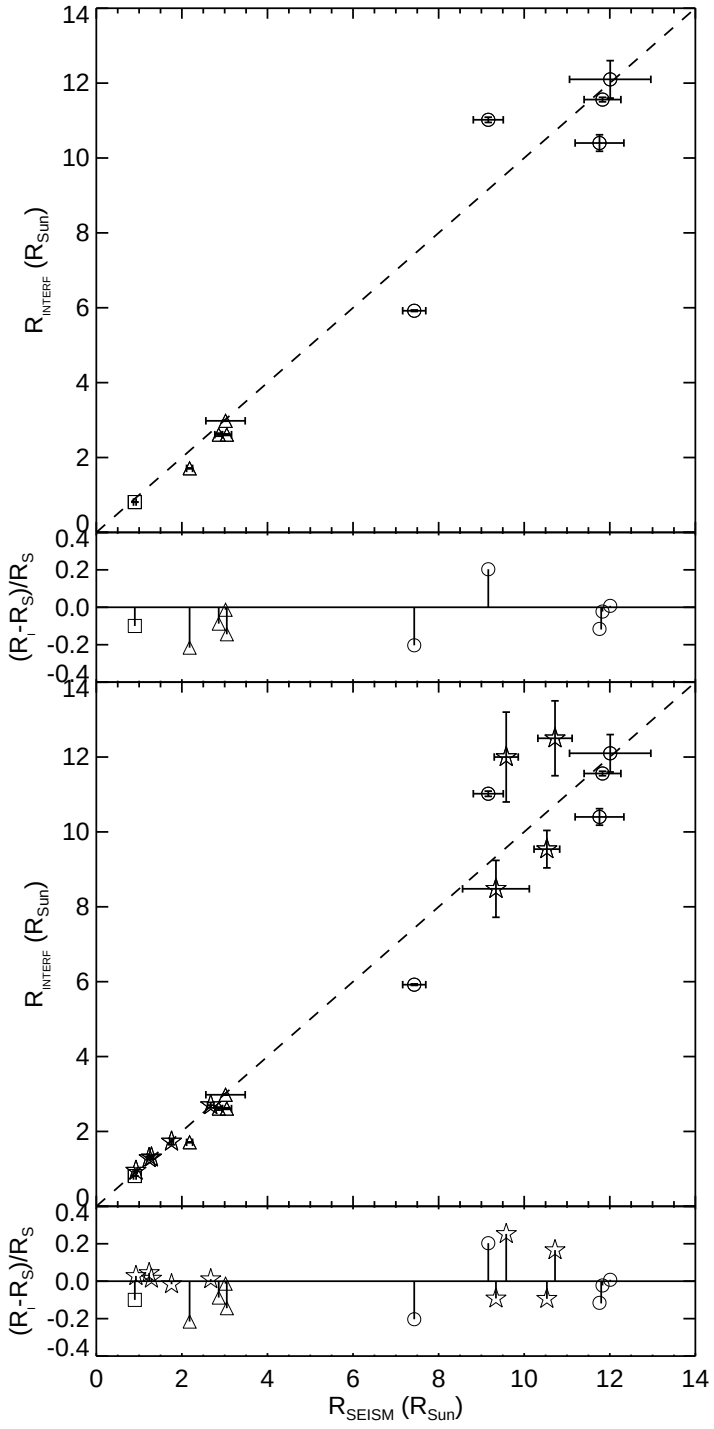

Fig. 4.— Comparison between interferometrically measured radii and those determined asteroseismologically listed in Table 4. The square represents the dwarf star, the triangles are subgiant stars, and the circles are giant stars. In the large bottom panel, the targets from Huber et al. (2012b) are added in as stars. The dashed line is the 1:1 ratio. The small bottom panels show the residuals to the fit normalized to the asteroseismic radii.

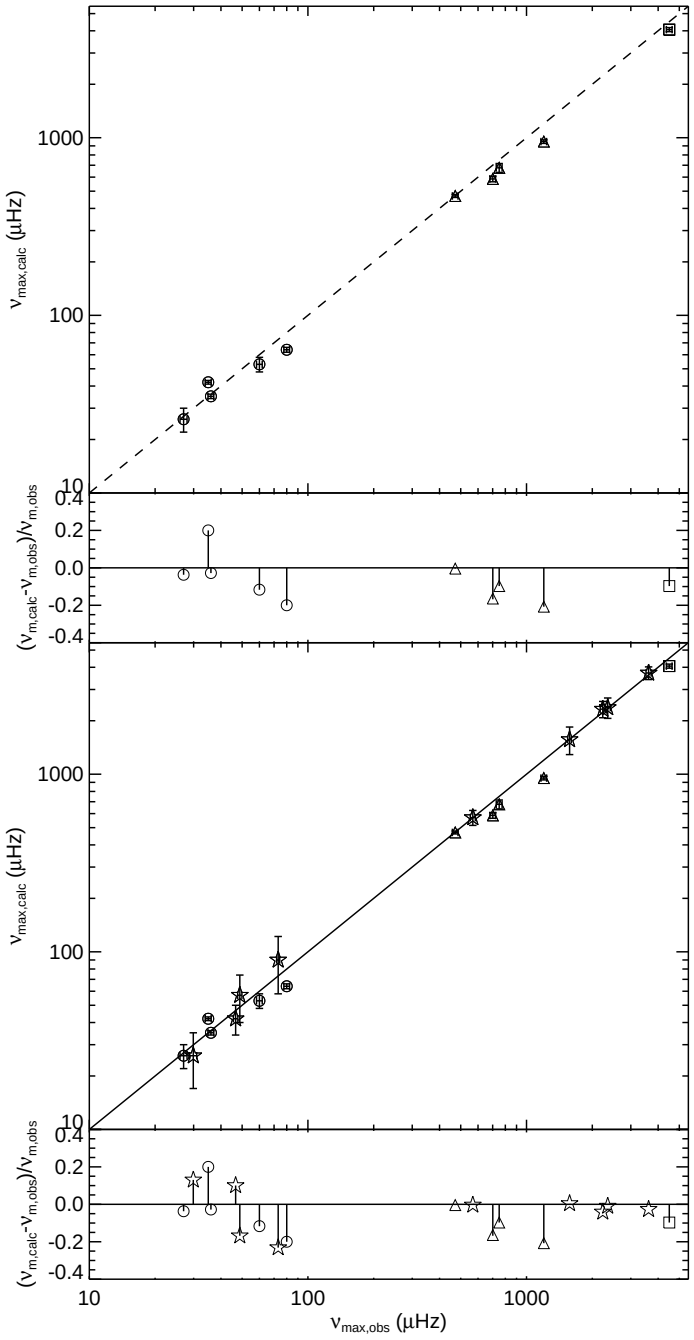

Fig. 5.— Comparison between the calculated and observed $\nu_{\rm max}$ values from Table 4. The symbols are the same as in Figure 4.